Thomas, R., Rericha, A., Pohl, W. L., Davidson, P. (2018): Genetic significance of the 867 cm−1 out-of-plane Raman mode in graphite associated with V-bearing green grossular. - *Mineralogy and Petrology*, *112*, 5, pp. 633—645.

DOI: http://doi.org/10.1007/s00710-018-0563-1

# Genetic significance of the 867 $cm^{-1}$ out-of-plane Raman mode in graphite associated with V-bearing green grossular

**Rainer Thomas[a] • Adolf Rericha[b] • Walter L. Pohl[c] • Paul Davidson[d]**

✉ Paul Davidson

Paul.Davidson@utas.edu.au

0000-0002-6129-0748

[a] Helmholtz-Centre Potsdam, German Research Centre for Geoscience – GFZ, Section 4.3. Chemistry and Physics of Earth Materials, Telegrafenberg, D-14473 Potsdam, Germany

[b] Alemannenstr. 4a, D-14612 Falkensee, Germany

[c] Austrian Academy of Sciences, Dr. Ignaz Seipel-Platz 2, 1010 Vienna, Austria

[d] ARC Centre of Excellence in Ore Deposits, University of Tasmania, Hobart 7001, Australia

**Keywords:**

Tsavorite

Green V-grossular

Graphite

Raman scattering

Fluid and melt inclusions

Sulfur

**Abstract** SE Kenya is the world's largest producer of green vanadium grossular gemstones (tsavorite). Samples from one of the mines near Mwatate, and of occurrences in Tanzania yielded remarkable new insights into the genesis of tsavorite. Graphite is intimately associated with V-grossular and is one of the keys to understanding its origin. In the course of this study we found five different types of graphite. Surprisingly, in one graphite type the "Raman-forbidden" and IR-active 867 $cm^{-1}$ band was observed. In this communication, we attempt to find an explanation for this unusual phenomenon. Additionally, our observations also address some of the issues pertaining to the origin of the green grossular-dominated rocks (grossularites), as well as the gem quality tsavorite crystals, since we propose that the anomalous spectroscopic behavior of the graphite is related to the unusual conditions during crystallization of both the grossular and graphite from a near-supercritical volatile- and sulfur-rich silicate melt. The massive green vanadium grossular contains abundant unequivocal crystallized melt inclusions, while the transparent gem quality grossular (tsavorite) displays only fluid inclusions. On the basis of inclusion studies we suggest that anatectic fluids originated in the peculiar evaporitic host lithology of the tsavorite deposits. Near peak metamorphic temperatures (~700°C) these liquids occurred as a supercritical volatile-rich "fluid/melt phase" characterized by complete miscibility between $H_2O$ and silicate liquid. Relatively dry liquid batches precipitated non-transparent green grossular, whereas wet batches segregated fluids that formed transparent tsavorite.

## Introduction

During the search for graphite references we studied hundreds of graphite crystals, including some genetically related to grossular and tsavorite from SE Kenya and Eastern Tanzania. Surprisingly we found that the normally infrared-active mode at 867 $cm^{-1}$ became Raman-

active, but only in these East African samples. In this contribution, we attempt to explain the origin of this unusual behavior of this graphite, which probably lies in the unusual paragenesis. The initial discovery of this anomalous graphite, and then the discovery of unequivocal melt inclusions in the massive grossularite (in contrast to Feneyrol et al. 2010; 2013; 2017) as the dominant inclusions, suggested a working hypothesis that green vanadium grossular in E-Tanzania and SE-Kenya originated from the fluid-rich, chemically unusual anatectic melt, not only from dehydration fluids as proposed by Feneyrol et al. (2017). Explaining this unusual spectrographic behavior, and testing this hypothesis was the motivation for this study.

Graphite belongs to the dihexagonal-dipyramidal class in the hexagonal crystal system. According to Dresselhaus et al. (1977) pristine graphite, which crystallizes in the $D_{6h}^{4}$ space group (Schoenflies), has twelve vibration modes: three acoustic modes ($A_{2u} + E_{lu}$), three infrared-active modes ($A_{2u} + E_{lu}$), four Raman-active modes ($2E_{2g}$) and two silent modes ($2B_{1g}$). In the first-order region of the Raman spectrum (1100-1800 $cm^{-1}$) the graphite band (G band) occurs at 1580 $cm^{-1}$. In poorly ordered carbon there are further bands: a broad and intense band at 1350 $cm^{-1}$ (D1 band), a weak band as a shoulder on the G band at 1620 $cm^{-1}$ (D2 band), and a very wide and weak band (D3) at about 1500 $cm^{-1}$. The transformation temperature of carbonaceous material into graphite, *sensu stricto* can be estimated to ± 50 °C in the range 330-650 °C using the D1, D2, D3, and G bands in the first order region (Beyssac et al. 2002) using the R2 peak area ratio D1/(G + D1 + D2). The temperature is calculated using the linear function T (°C) = -445R2 + 641. However, by including hydrothermal and magmatic graphite to the Beyssac metamorphic data base, and using an Arrhenius plot the formation temperature of magmatic and hydrothermal graphite can be estimated up to 780 °C (see Hurai et al. 2015) according to the equation

$$10{,}000/(t + 273.15) = 9.82794 + 9.5697 * R2 \qquad (1)$$

where t is temperature in °C.

Green gemstone quality garnets ('tsavorite') in East Africa are grossular crystals colored by reduced $V^{3+}$ and $Cr^{3+}$, with the general formula $Ca_3(Al,V,Cr)_2(SiO_4)_3$ (Feneyrol et al. 2013). Host rocks, quartz veins and crystallized melt inclusions in massive green grossular contain graphite. Isotopic and chemical data characterizing the graphite have been published previously (Suwa et al. 1996; Arneth et al 1985). The purpose of this study is a mineralogical Raman investigation of graphite types, and of melt, solid and fluid inclusions in green V-grossular. Together with rapid quench experiments on melt inclusions of the latter, improved understanding of the origin of green V-garnet and the associated graphite is expected.

**Geological setting**

Tsavorite (the trade name of gemstone-quality emerald-green grossular) in East Africa is exploited in the Mozambique Belt, which is part of the East African Orogen (Fritz et al. 2013) that formed along the present African coast in the Neoproterozoic Era. The orogen evolved from rifting and break-up of Supercontinent Rodinia, which had been finally welded at ~1000 Ma, to an oceanic stage called the Mozambique Ocean. Anhydrite bearing precursors of the later tsavorite host rocks (Feneyrol et al. 2017) were part of rift and passive margin sediments with intercalated bimodal volcanics (Pohl et al. 1979). Rifting was followed by prolonged subduction, nappe stacking, welding of microcontinents and volcanic arcs, and final collision. The gemstone-hosting rocks are part of the meta-sedimentary nappes of the Eastern Granulite Province (Tenczer et al. 2013). Deformation and metamorphism in the Mozambique Belt are peculiar because a first orogeny (called "East African") between 650 and 620 Ma included a long period of high T and P (Tenczer et al. 2011). A second orogenic episode ("Kuungan" or "Malagasy") took place between 580 and 550 Ma (Tenczer et al. 2013), marking the final amalgamation of Supercontinent Gondwana.

Tsavorite gemstones in SE Kenya occur along strike of the Kurase Group, a metasedimentary unit of siliclastics, carbonates and volcanics. A metapelitic member of the group extends over a distance of ca. 100 km, punctuated by about two dozen gemstone mines (Martelat et al. 2017: their figure one and figure two). The northern part is covered by the Geological Map of the Mwatate Quadrangle (1:50,000; attached in Pohl et al. 1979). Tsavorite occurrences in Tanzania are found in similar rocks (Feneyrol et al. 2017: their figure two) but mines are less productive (USGS 2015a, 2015b). Rocks of the Kurase Group were deformed and metamorphosed in the East African orogeny. In SE Kenya, peak conditions of the upper amphibolite facies were reached (~7 kbar and ~700 °C: Pohl et al. 1979). Typical of amphibolite facies rocks, migmatites and metamorphic mobilizates such as pegmatites and quartz veins are ubiquitous in the region; granites are absent. Pegmatites and quartz veins occur in clastic metasediments (paragneiss and quartzites) but rarely intrude the metapelitic (quartz, feldspar, sillimanite, kyanite), graphitic, carbonatic, and evaporitic (Ca-scapolite-bearing) schists and gneisses hosting green grossular and gem tsavorite (Pohl et al. 1979, Pohl and Horkel 1980); in one mine only, anhydrite stringers have been observed (Feneyrol et al. 2013).

Generally, the origin of the vanadium grossular is attributed to a peak of prograde metamorphic dehydration and partial melting (Pohl et al. 1979, Martelat et al. 2017). However, the correlation with the dates of the regional tectono-metamorphic evolution remains uncertain. Attempts to date the formation of grossularites with different rock, minerals and isotope systems (Feneyrol et al. 2017: vanadium grossular by Sm-Nd; Martelat et al. 2017: zircon, monazite, rutile by in situ U-Th-Pb, mica by 40Ar/39Ar) resulted in dates of 615-600 Ma, which deviate from both main orogenies mentioned above. Possibly, these dates are due to disturbances such as metamict zircons and/or resetting of isotope systems by later events (Zhang et al. 2017). Pohl et al. (1979) report that in an aeroradiometric survey (by Canadian International Development Agency, unpublished) the graphite-rich host rock

package of the V-grossularites produced U/Th anomalies. Zircons are rich in U and Th, and monazite from these rocks contains up to 5.3 wt% Th and 4.6 wt% U (Martelat et al. 2017). Partially or totally reset ages of the so-called “pan-African” group ranging down to 450 Ma reflect a tectono-thermal overprint in wide parts of Africa known since Cahen et al. (1984).

## Samples

For comparison, and to gain additional information, three sample sets were used. One was from the South Kenyan Mwatate region, and two from the Merelani region in Tanzania. Massive coarse-grained bright green vanadium grossular material (sample 1) was collected from an underground exposure in the Scorpion mine (Fig. 1), located in the South Kenyan Mwatate region (Pohl et al. 1979, Bridges and Walker 2014) - see also Martelat et al. (2017, their figures 1 and 2). Sample 1 was taken from veins that formed in the lateral pressure shadow of a large, elliptically deformed, homogeneous, isotropic and tough body, possibly a metamorphosed diagenetic calcareous concretion (electronic supplementary material, Fig S1b). The veins formed in graphite schist of the tsavorite horizon. In this space, small pockets and veinlets of quartz and calcite enclose non-transparent green grossular and transparent gem material (tsavorite). Less frequently, gem-bearing pockets and veinlets display graphite, mostly in coarsely bladed pockets, rims or veinlets in contrast to the smaller (< 1 mm) flakes dispersed in the host rock.

The material (see electronic supplementary material, Fig. S1) contains graphite crystals in five texturally different positions. In addition to graphite, the following mineral inclusions were observed: calcite, quartz, anorthite, scapolites (marialite, meionite), diopside, zoisite, violarite [$Fe^{2+}Ni_2{}^{3+}S_4$], hessite [$Ag_2Te$], tennantite [$(Cu,Ag,Zn,Fe)_{12}(As,Sb)_4S_{13}$], arzakite [$Hg_3S_2(Br,Cl)_2$] (see electronic supplementary material, Figs. S2, S6) and claudetite

[$As_2O_3$] (S9). In the center of the studied green grossular aggregates or fragments there are symplectitic, or graphic, intergrowths of zoisite, and diopside, with small amounts of quartz and calcite. Subordinate, rounded titanite and zircon crystals occasionally occur throughout the sample.

Samples of Tanzanian green grossular and gem tsavorite are from the mining area of Merelani (Feneyrol et al. 2017: their figure two). Sample 2 is massive coarse-grained green grossular which is intensely brecciated.

For comparison, we investigated tsavorite crystals of gemstone quality from Merelani, Tanzania (sample 3; see electronic supplementary material, Fig. S1c). The exact site of origin remains unclear. This tsavorite contains graphite inclusions, as well as attached graphite crystals. Solid sulfide mineral inclusions are absent, but skeletal crystals of diopside are common inside the tsavorite crystals.

## Methods

### Micro-Raman spectroscopy

Raman spectra were recorded with a Jobin-Yvon LabRam HR800 spectrometer (grating: 1200 and 2400 gr/mm), equipped with Rayleigh filters, polarizer, an Olympus optical microscope, and a long-working-distance LMPlan 100×/0.80 objective for high-resolution work. We used the internal 633 nm, and primarily the 514 and 488 nm excitation of a Coherent Ar+ laser Model Innova 70C, generally with a power of about 4.5 mW on the sample.

The spectra were collected at a constant laboratory temperature (20 °C) with a Peltier-cooled CCD detector, and the position of the Raman bands was controlled and corrected using the principal plasma lines in the Argon laser. The differences between

recommended and measured positions of the plasma lines in the fingerprint spectral region are not larger than 0.6 $cm^{-1}$. For the determination of the background and the peak position we used the LabRam HR800 LabSpec 5 routine. Representative Raman spectra of all of the mineral phases described in this study are provided in the electronic supplementary material. For the identification of the mineral phases with Raman spectroscopy we used the RRUFF database together with the CrystalSleuth interface (Lafuente et al. 2015).

**Hydrothermal rapid-quench homogenization experiments**

Pieces of double-polished plates of tsvorite (500 µm thick) were placed into an Au-capsule (5 × 30 mm) with a fixed amount of pure water. The inclusions were re-melted at 700 °C or 750 °C at a pressure of 2 kbar, using the conventional hydrothermal rapid quench technique. The run time of the unbuffered experiments was 24 hours. After the run, the sample was quenched isobarically. The quench rate is 100 °C/s. Run products were studied by microscope under immersion oil (see Veksler and Thomas 2002).

**Microthermometric and Raman spectrometric measurements of the aqueous inclusions**

Microthermometric measurements were performed using a LINKAM THMS 600 heating and freezing stage, together with a TMS 92 temperature programmer and a LNP 2 cooling system mounted on an Olympus microscope. The stage was calibrated with synthetic fluid inclusions (SYNFLINC) and melting points of different melting standards. All measurements were performed in an argon atmosphere, to guard against oxidation. The standard deviation depends on absolute temperature and is always less than ± 2.5 °C for temperatures greater 100 °C, and 0.2 °C for cryometric measurements less than 20 °C. Samples were 300µm thick, doubly polished tsavorite-chips. For solutions with significant amounts of carbonates, we used

the isotherms of $Na_2CO_3$-$H_2O$ (Makarov 1933) for cryometric measurements, and the cryometric criteria of Borisenko (1977) to determine the salinity expressed in % (g/g) equivalents. The carbonate concentrations determined by Raman spectrometry (see Thomas and Davidson, 2012) are $Na_2CO_3$ % (g/g) equivalent concentrations, because according to Oliver and Davis (1973) the carbonate frequencies are virtually independent of alkali metal cations (Li, Na, K, Rb, Cs). According to Nývlt (1977) the solubility of the main alkali carbonates (Li, Na, K) at 20 °C is 1.31, 18.1, and 52.5 % (g/g), respectively.

### Experimental formation of La-intercalates in graphite

A simple test tube experiment was performed to determine if the formation of La-intercalates could generate the observed anomalous 867 $cm^{-1}$ band in graphite. Graphite powder (natural coarse-crystalline graphite from Sri Lanka) and analytical-pure La-carbonate powder were mixed in the weight ratio of C : La = 10 : 1 and intensively ground in an agate mortar. The untreated graphite from Sri Lanka shows no indication of the 867 $cm^{-1}$ band. The studied graphite plates had a dimension of about $\leq 5 \times 0.2$ µm

## Results

### Anomalous Raman spectrographic behavior of graphite

A total of five texturally different types of graphite crystals have been identified during the study:

Graphite-I – Macroscopic graphite attached to the grossular crystals (electronic supplementary material, Fig. S1e).

Graphite-II – Microscopic well-formed, generally lathlike graphite crystals inside green grossular (Fig. 2a).

Graphite-III – Graphite similar to Graphite-II, however, disintegrated into mosaics, decorated with several sulfide minerals (mostly arzakite) - (Fig. 2a).

Graphite-IV – Small graphite crystals (~10 μm in diameter) suspended in fine-grained zones inside the green grossular containing zoisite, grossular, anorthite, quartz, diopside, and fersmite [ $(Ca, Ce, Na)(Nb, Ti)_2(O, OH, F)_6$] inclusions in titanite. according to the Raman studies, apart from the size, this graphite resembles the graphite-I.

Graphite-V – Graphite as a daughter crystal in melt inclusions.

In examining the differences in graphite types Raman spectroscopy is a powerful technique, allowing quite small changes in the structural morphology to be detected (Dresselhaus et al. 1977, Reich and Thomsen 2004). The different graphite crystals were studied with Raman spectroscopy: two typical Raman spectra of graphite-I and graphite-II are displayed in Fig. 3, with the Raman bands around 1360, 1580, and 1620 $cm^{-1}$.

The geothermometer proposed by Beyssac et al. (2002) gives a temperature of 640 °C for graphite-I. This temperature corresponds to the maximum temperatures conditions reached during regional metamorphism. The near-complete absence of the D1 band is typical for this graphite-I. A relatively strong D1 band with slightly varying intensity can be seen in the Raman spectrum of graphite-II. The calculated crystallization temperature of graphite-II exposed at the sample surface was 530-460 °C. However, according to Beyssac and Lazzeri (2012) this large difference of around 100 °C can be attributed to structural defects in the graphite produced by the grinding and polishing. Measurements on graphite in the same crystal a few micrometers deep in the grossular matrix confirmed this by giving a calculated temperature of 640 °C. Graphite-IV and graphite-V yielded temperatures of 600 °C and 623 °C, respectively.

In contrast to graphite-I, -III, IV and -V, however, graphite-II exposed on the sample surface shows a clear and sharp band at 867 $cm^{-1}$, which is IR active and should normally be Raman-inactive (Fig. 2b). From 15 measurements (laser wavelength 514 nm, power 4.5mW on sample) a position of 866.6 ± 0.4 $cm^{-1}$ with a FWHM = 2.7 ± 1.0 $cm^{-1}$ was determined (FWHM – full width at half-maximum). When laser wavelengths of 488 and 633 nm are used, this position remains almost identical. The 633 nm laser produces a value of 866.3 ± 0.6 $cm^{-1}$, FWHM = 1.9 $cm^{-1}$ (n = 10 measurements). The intensity of this band depends strongly on the polarization: in analogy to Kawashima and Katagiri (1999, 2002) the highest intensity was found with the incident light polarized perpendicular to the graphite plane ($E \perp c$) and is reduced to nearly zero parallel to it ($E \parallel c$).

The intensity of the 867 $cm^{-1}$ band is only 1/30 of the G band and can thus easily be overlooked in the Raman scattering experiments. However, this band is not visible in graphite beneath the garnet surface. It is also not discernible in polished graphite-I, therefore its formation by mechanical impact during grinding and polishing can be dismissed. The influence of the strong grossular band at 879 $cm^{-1}$ should also be disregarded, since a graphite layer of several nanometers on grossular completely suppresses this band.

To see whether the observation of the Raman "forbidden 867 $cm^{-1}$ band" only applies to the sample from Kenya, another sample (sample 2) from a similar deposit in Tanzania was examined. In this sample we also observed the sharp band in the type-II graphite, but not in the other graphite types (see Fig. 3).

Graphite-II and -III are directly physically adjacent, differing only texturally – and they should have grown under the same conditions. We hypothesise that small differences in concentrations of intercalation compounds (e.g. arzakite and/or lanthanite) and the disruption of the crystal structure during mosaic texture formation have led to great differences in the behavior of the two different graphite forms.

**Melt and fluid inclusion studies in East African grossularite**

While studying the anomalous Raman spectrographic behavior in graphite associated with grossular garnet in grossular dominated rocks (grossularites), unambiguous melt inclusions in grossular crystals were observed. Given the current uncertainty as to the origin of these rocks an extensive study was carried out to see if there was any link between their origin and the anomalous Raman spectrographic behavior in the associated graphite. Typical un-homogenized melt inclusions are shown in Figs. 4, 5, and 6.

Abundant crystallized melt inclusions (Fig 4a) are typical of sample 1 (grossular from Kenya), according to Raman spectroscopy containing mostly calcite, quartz, and scapolite (meionite [$Ca_4[Al_6Si_6O_{24}]CO_3$]), trilithionite [$KLi_{1.5}Al_{1.5}AlSi_3O_{10}F_2$] and up to 50 % (vol/vol) of a fluid sub-phase ($H_2S + CO_2 + H_2O$). In larger melt inclusions we detected native sulfur in high concentrations [up to 10 % (vol/vol)], claudetite [$As_2O_3$] as small solid globules and $H_2S$ as the dominant liquid phase. The mineral phases titanite, diopside, cerianite-(Ce) [$(Ce^{4+}, Th)O_2$], koenenite [$Na_4Mg_9Al_4Cl_{12}(OH)_{22}$], riomarinaite [$BiSO_4(OH) \cdot H_2O$], and the V-bearing (6.6 % (g/g) $V_2O_5$) mineral saneroite [$Na_2(Mn^{2+}, Mn^{3+})_{10}(Si_{11}, V^{5+})O_{34}(OH)_4$] and the V-mineral patrónite [$VS_4$] (~28 % V (g/g)) are all present but subordinate or rare in the sulfur-rich melt inclusions (see electronic supplementary material Fig. S9).

For extremely volatile-rich melt inclusions the quenching rate we could achieve (~ 100 °C/min) is usually insufficient to prevent phase seperation during cooling. From rapid quench experiments (700 and 750 °C, 2 Kbar, 24 hours) we found melt inclusions composed of glass, liquid, and vapor, with phase relations corresponding to critical or near-critical conditions (see Thomas and Davidson 2016). The estimated bulk water content is about 30 % (g/g) (see Fig. 5a). Experiments run at 700 °C homogenised only some of the smallest MI, implying that 700 °C corresponds to the trapping temperature, which is consistent with the

estimates from geothermometry (Pohl et al. 1979). In addition to the silicate melt inclusions there are also sulfur-rich melt inclusions, containg solid sulfur and graphite, liquid $H_2S$ and $H_2S$-vapor at room-temperature (Fig. 5b). Figures 5d and 5e show a pseudosecondary trail of small melt inclusions with highly variable phase composition. Most inclusions contain a sulfur daughter phase, some to very high concentrations.

Fluid inclusions are very rare – if present they are generally secondary in origin, often arranged as halos around larger melt inclusions, probably representing decrepitation halos formed during initial cooling by aqueous fluids injected into cracks formed during decrepitation, and subsequently partly healed by grossular crystallizing from the grossular saturated fluids. Rare primary fluid inclusions do occur and contain a $CO_2$ and carbonate-rich fluid phase, a bubble, and a daughter crystal of calcite.

The melt inclusions in massive green grossular from Tanzania (sample 2) are similar to the material from Kenya. Raman bands of native sulfur are often observed. This implies very high sulfur activity during the crystallization of green grossular from the silicate melt at about 700 °C. That is also indicated by the coexistence of occasionally extremely sulfur-rich melt inclusions in this sample, at room-temperature containing a large solid sulfur globule [up to 10% (vol/vol)], liquid $H_2S$ and a $H_2S$ vapor phase with only traces of $N_2$ (see Fig. 6).

For comparison, we investigated tsavorite crystals of gemstone quality (sample 3) from a deposit in the Merelani Mine region, Tanzania. The exact site of origin remains unclear. In contrast to the other two samples, the crystals contain only fluid inclusions and no melt inclusions. Large primary fluid inclusions contain small daughter crystals. From the inclusion association we conclude that the samples crystallized at different physicochemical conditions: samples 1 and 2 from a melt-dominated system, whereas sample 3 indicates a fluid-dominated system during gem crystallization.

The fluid inclusions in sample 3 (transparent tsavorite crystals from Tanzania, Fig. 7) homogenize into either the fluid or vapor phase at 350 ± 5 °C (n = 10), implying that the

inclusions were trapped directly on the liquid-vapor curve. The eutectic melting occurs at -3.1 °C. According to Makarov (1933) and Borisenko (1977), these temperatures indicate $Na_2CO_3$ concentrations of 5.0 % (g/g) and NaCl concentrations of 2.2 % (g/g). Larger fluid inclusions in the tsavorite crystals are relatively rare. They contain an aqueous solution with two different daughter mineral phases. The first one forms colorless isometric platelets, probably natron [$Na_2CO_3 \cdot 10H_2O$], with a melting temperature of 30 ± 0.7 °C. With Raman spectroscopy (see Oliver and Davis 1973) we estimate an alkali carbonate concentration of 3 mol/l $CO_3^{2-}$ and significant amounts of dissolved $CO_2$. Given interference from the strong luminescence at wavelengths >1500 $cm^{-1}$ use of the $H_2O$-bands as reference was not possible. According to Nývlt (1977), the melting temperature of the first daughter phase (natron), gives a concentration of 28.7 % (g/g) $Na_2CO_3$ corresponding to 2.7 mol/l, which roughly confirms the value estimated by Raman spectroscopy. The other colorless and highly refractive daughter mineral phase [about 2.4 % (vol/vol) average, with a maximum of 6.8 % (vol/vol)] is insoluble up to the homogenization temperature. Given the dominant intense sharp bands at 1076, 1080, and 1091 $cm^{-1}$, the weak Raman band at around 750 and 301 $cm^{-1}$, the strong doublet at 104 and 118 $cm^{-1}$, and the formation of graphite directly on the daughter mineral phase during the laser irradiation, we interpret this second colorless daughter mineral with the intermediate index of refraction $\beta >> 1.658$ (in relationship to calcite), as a REE-bearing- or REE-carbonate mineral – see the electronic supplementary material Fig. S8 and Frost et al. (2013). For the exact identification of the mineral further studies are required.

In our search for the origin of the anomaly 867 $cm^{-1}$ band in the Raman spectrum of graphite related to the green grossular from Kenya and Tanzania we have discovered two apparently parallel melt inclusion systems, one very $H_2O$-rich, similar to previously described MI from pegmatites, the other is a previously undescribed and very unusual silicate melt-volatile system in which sulfur and hydrogen sulfide are the determining constituent of the system (see Fig. 4). In some cases sulfur almost completely replaces water. Moreover, this

system also shows clear indications of liquid-liquid immiscibility according to the scheme S-rich silicate melt into $H_2O$-rich silicate melt and a complex melt or fluid S-$H_2S$-HS-$H_2S_n$ system. The extremely sulfur-rich inclusions were probably formed by liquid-liquid immiscibility from low-viscosity silicate melt. Note that melt-melt immiscibility need not be a single-stage process, as each immiscible phase may itself undergo melt-melt immiscibility as it evolves independently down temperature and pressure. Although fascinating, the thermodynamically unusual behavior of hydrogen sulfide in molten sulfur at high temperatures and pressures and its significance for the liquid-liquid immiscibility process were outside the scope of this paper.

## Discussion

### Anomalous Raman spectrographic behavior of graphite

Up to five different types of graphite are associated with vanadium grossular from Kenya and Tanzania and are characterized by the typical spectrum of highly oriented graphite with strong bands at about 1581 and 1330 $cm^{-1}$. Using three different laser wavelengths, we observed in one type (graphite-II) a very sharp peak at 867 $cm^{-1}$. The position is more or less independent of the wavelength used. The intensity of this band is, however, only 1/30 of the G band and can thus easily be overlooked. According to Nemanich et al. (1977) and Dresselhaus et al. (1977), there is an infrared-active mode at this position, and it should normally be "forbidden" in the Raman spectrum. Further studies have shown that the intensity of this band depends strongly on the polarization.

In this contribution, we hypothesize that intercalation of S and/or REE into the graphite crystal structure, along with reversible stress associated with the formation of the

mosaic texture of type III graphite may explain why the normally infrared-active mode becomes Raman-active. Our observations are consistent with the model given by Feneyrol et al. (2013) in which the tsavorite crystals were formed during prograde metamorphism of sedimentary sequences, characterized by evaporitic minerals such as anhydrite and scapolite with a high concentration of carbonic and sulfuric material (see also Warren 2006, chapter 3). Schematically, in the presence of graphite sulfate sulfur is reduced as shown in the following equations:

$$CaSO_4 + C + H_2O \leftrightarrow CaCO_3 + O_2 + H_2S \text{ and} \quad (2)$$

$$H_2S + ½\ O_2 \leftrightarrow H_2O + S \quad (3)$$

At high temperatures (650 – 700 °C) such systems are highly reactive and corrosive (Gorbaty and Bondarenko 1998).

Graphite-II and -III in the green vanadium grossular from Kenya are found in very close proximity to each other within the crystals. Graphite-III is characterized by a mosaic-like texture with some sulfide mineral precipitations on the mosaic grain boundaries – graphite-II is free of such precipitates and mosaic texture. Given the high $S/H_2S$ partial pressure during crystallization of the graphite at magmatic P-T-conditions, it seems reasonable that the large molecule $S_8$ would be broken into the smaller chain species $S_2$, which can intercalate into the expanded graphite. With cooling to room temperature the intercalated $S_2$ may recombine to form cyclo-$S_8$ (Zheng et al. 2014), and the intercalated sulfur changes the symmetry of graphite (Yang et al. 2001). With decreasing temperature and pressure, the stability of these graphite intercalation compounds declines, and reactive sulfur/$H_2S$ may be expelled and could react with any active cations present, forming stable sulfides such as pyrite, arzakite, and others. After that, the graphite no longer shows the structural anomaly. We suggest that this results from the sulfur intercalates having been removed completely in the open space-grown graphite-I and partially in graphite-II and -III. This process would also explain the mosaic texture, as the escape of the intercalation

compounds would necessarily disrupt the graphite crystal lattice. In contrast, graphite crystals encased in green grossular that does not show mosaic texture (Graphite-II), does show the anomalous 867 $cm^{-1}$ band, presumably due to have retained the structural anomaly.

Since these Tanzanian tsavorite crystals contain no sulfide mineral inclusions, the formation of the band at 867 $cm^{-1}$ cannot be attributed to damage to the graphite lattice through sulfur alone. There are no sulfide minerals in the hydrothermal gem-grade tsavorite, in contrast to massive grossularite, and we have never found sulfur in the fluid inclusions. Given the high REE concentration in the primary fluid inclusions indicated by the REE-bearing- or REE-carbonate daughter mineral, currently of unclear composition, the appearance of other REE minerals in the fluid inclusions, and the presence of cerianite-(Ce) and fersmite as a mineral inclusions in green grossular, we speculate that primary REE intercalates in graphite were formed (see for example Shikin et al. 2000; Chen and Stimets 2014). This is justified by the experimental result that by grinding graphite together with La-carbonate or $NdF_3$ (10 : 1) in a motar, the graphite clearly displays the 867 $cm^{-1}$ band (see Fig. 8). Note that according to Feneyrol et al. (2017) the $Sm^{3+}$ and $Nd^{3+}$ concentrations in the primary tsavorite crystals are high (up to 18.5 and 14 ppm, respectively), indicated by the extremely strong luminescence background in the 633 nm Raman spectrum (see Fig. 9).

An alternative explanation is that this band has been generated by directional differential stress during the trapping of graphite in the tsavorite as a result of the very different expansion coefficients of the two minerals. However, since this greater stress is reduced when the sample is polished it suggests that whatever the cause, the process is non-reversible, and the symmetry change, once locked-in, does not revert.

**Origin of the East African grossularite**

Kenyan green grossular samples display melt inclusions (Fig. 4), primary fluid inclusions are almost absent. This observation is inconsistent with the generally proposed model of a formation from metamorphic aqueous fluids (Feneyrol et al. 2013 and 2017) and requires a new model. Giuliani et al. (2015, 2017) provided the first suggestions as to a possible role of metamorphic liquids (salt melts) in gemstone formation from evaporitic host rocks. In SE Kenya, melt formation is probably related to the phase of dehydration, anatexis and fluid expulsion affecting the volcano-sedimentary rock suite during the East African Orogeny (ca. 640 Ma).

Graphite in the host rocks displays an isotopically biogenic signature, possibly with admixture of carbon derived by silication of calcite marbles (Feneyrol et al. 2013), and may constitute ≈ 20% (g/g) of the rock (Arneth et al. 1985). Formed in saline lagoons or mudflats (Warren 2006), organic substances (e.g. *algae*) were deposited with pelites; from the kerogen, oil and gas ($CH_4$) must have been generated and expelled during diagenesis, followed by graphitization during metamorphism. Reacting with organic matter and/or hydrocarbons, anhydrite would have contributed to formation of $H_2S$. As a diagenetic collector of vanadium and other trace metals, the organic substance and its derivative kerogen/graphite are most probably the main source of V for green grossular formation. Metamorphic liquids and fluids are thought to have extracted the elements that formed and gave colour to green grossular and the tsavorite gems (Pohl et al. 1979, Feneyrol et al. 2013). At high-grade metamorphism, the formation of carbon-bearing liquids/fluids is common (Luque et al. 2014).

We suggest that as at Round Hill, near Broken Hill, Australia (White et al. 2004), garnet bearing leucosomes may be interpreted as evidence of in situ melts, with the garnet representing the residuum, whereas coarse-grained pegmatite-like garnet-poor leucosomes would represent segregated and migrated melt (Pawley et al. 2015). These authors report that often, large garnets are left behind as the leucosome-forming liquid around them drained away. In the East African context the quartz-calcite-grossular veinlets (e.g. star in fig. 1) are

the garnet bearing leucosomes. The removal of the fluid/melt from the garnets prevents the rehydration reactions that could cause the garnet to break down in retrogression. This may explain the observation that some tsavorite nodules have kelyphitic shells whereas others display no trace of hydrous alteration.

The presence of melt inclusions in the grossular is quite convincing evidence that they crystallized from a high temperature (~700 °C) silicate melt. The extremely volatile-rich melt inclusions described imply that this "melt" was a supercritical volatile-rich "fluid/melt phase", characterized by complete miscibility between $H_2O$ and silicate liquid (Shen and Keppler 1997, Thomas and Davidson 2016). In this context the presence of abundant granitic pegmatites in the adjacent clastic sediments is significant. Some studies (e.g. Thomas and Davidson 2016) propose that granitic pegmatites form from extremely volatile-rich silicate melt/fluids [often ~50 %(vol/vol) volatiles] and that many unusual features of such pegmatites are a consequence of their unusual volatile-rich chemistry. There seems to be a clear implication that the grossularites and the granitic pegmatites may be a similar response in adjacent but contrasting rock-types. This supercritical phase is marked by extremely low density, viscosity and surface tension, high diffusivity, reactivity, and mobility. Near critical conditions, the solubility of some elements such as REE, Cr and V is extraordinarily high. We note the presence of high concentrations of these elements in tsavorite and green grossular-rich rocks, V is required as a colouring agent, and some REE and S are required to explain the anomalous spectrometry of the graphite.

The discovery of often very sulfur-rich MI in the grossular, described in the results, is interesting. Rankin et al. (2013) described sulfur and liquid hydrogen sulfide rich fluid inclusions in tanzanite from Merelani, Tanzania, and the present study suggests that extremely S-rich melt systems can be generated during metamorphic high-temperature and high-pressure processes from anhydrite-bearing evaporites. Elsewhere, the possibility of extremely sulfate-

rich, magmatic systems has been described, for example by Naumov et al. (2008), Thomas and Davidson (2017), and Hurai et al. (2017). The possible overlaps are intriguing.

The behavior of the extremely high sulfur and sulfur-compound concentration, or their activity at temperatures around 600 to 700 °C is completely unknown. According to Gorbaty and Bondarenko (1998), in the presence of water, such systems are highly corrosive and can show unusual behavior near the critical isochore during heating or cooling, connected with very strong structural fluctuations.

The contrasting melt versus fluid inclusion populations in grossular and tsavorite indicate that the crystallization of green vanadium grossular occur in two different regimes. Initially in a sulfur-rich supercritical silicate liquid under upper amphibolite facies P-T conditions in a regime of partial melting, and then by re-crystallization under a hydrothermal fluid regime at moderate temperatures and pressures.

## Conclusions

Traditionally, Raman experiments on graphite have mostly been performed at the wavelength range >1000 $cm^{-1}$ (see also Zheng et al. 2014). The present study has shown, however, that the infrared-active mode at 867 $cm^{-1}$ can become Raman-active, if for example, the dimension of the c-axis increases by insertion of intercalation compounds into the graphite, whereby the inversion symmetry of graphite is disturbed. The study in this extended range can give important information as to the interaction of the growing graphite with the surrounding media. We suggest that the strong enrichment of REE and/or sulfur in graphite and green vanadium grossular can produce the reversible formation of intercalation compounds in graphite, producing the unusual Raman characteristics in cases in which the intercalation compounds are not removed.

We suggest that at peak metamorphic conditions, within the evaporitic tsavorite host rocks at ~700 °C, a small volume of supercritical volatile-rich alkaline "fluid/melt phase" (*sensu* Thomas and Davidson 2016) was generated. In the clastic metasediments (paragneiss and quartzites) and felsic and mafic meta-volcanics true granitic pegmatites are abundant, but are absent in the tsavorite-hosting beds of evaporitic graphite-sillimanite-scapolite schists, implying that the grossularites and the granitic pegmatites may be a similar response in adjacent but contrasting rock-types. The green grossular and tsavorite could thus represent the product of parental melts (*sensu* Pawley et al. 2015) developed in the schists.

The presence of abundant melt inclusions, and the near-absence of fluid inclusions in non-transparent green vanadium grossularite confirm the involvement of an anatectic water-rich melt/fluid in the sense of Thomas and Davidson (2016), but transparent gem-quality tsavorite likely crystallized from an exsolved alkali-rich fluid evolving from volatile-rich melt/fluid. These observations complement the comprehensive studies published by Feneyrol et al. (2010, 2013), which are based only on fluid inclusions.

In conclusions, it should be emphasized that our initial aim was to solve the open questions related to the origin of the "Raman-forbidden" and IR-active 867 $cm^{-1}$ band in graphite from a well-known paragenesis. We note that our proposal as to the mechanism is tentative, and the nature of the intercalation elements remain to be positively identified by more sophisticated methods. However, that investigation broadened into consideration of the origins of the grossular dominated rocks themselves, and has increased the spectrum of new questions regarding to the unusual chemistry of the complex silicate melt-sulfur-carbon-$H_2O$-system. Furthermore, although the latter is only touched on, we hope it will bring new possibilities into geochemistry and especially into the inclusion research.

**Acknowledgments** The authors thank Patrick Arkfeld from the Arkfeld Minerals (Carlsbad, California, USA) for providing the tsavorite crystals from Tanzania, and the management of

Scorpion mine, Kenya, for cobbing waste. We thank Elena Badanina and Hans-Peter Nabein for the handling of the rapid quench experiments at GeoForschungsZentrum Potsdam. We also wish to thank Vratislav Hurai and Reinhard Kaindl for their helpful and constructive reviews, and Anton Beran as well as Lutz Nasdala for valuable suggestions. Our thanks also to Bob Downs for useful information regarding Raman spectra of lanthanite-(Nd) in the RUFF database.

## References

Arneth JD, Schidlowski M, Sarbas B, Georg U, Amstutz GC (1985) Graphite content and isotopic fractionation between calcite–graphite pairs in metasediments from the Mgama Hills, Southern Kenya. Geochim Cosmochim Ac 49:1553–1560

Beyssac O, Coffé B, Chopin C, Rouzaud JN (2002) Raman spectra of carbonaceous material in metasediments: a new geothermometer. J Metamorph Geol 20:859-871

Beyssac O, Lazzeri M (2012) Application of Raman Spectroscopy to the study of graphitic carbons in the Earth Sciences. EMU notes in Mineralogy, Vol. 12, Chapter 12, 415-454

Borisenko AS (1977) Cryometric technique applied to studies of the saline composition of solution in gaseous fluid inclusions in minerals. Geol Geofiz AN SSSR SO 8:16-27 (in Russian)

Bridges B, Walker J (2014) The discoverer of tsavorite – Campbell Bridges – and his Scorpion mine. The Journal of Gemmology 34:230–241 http://dx.doi.org/10.15506/JoG.2014.34.3.230

Cahen L, Snelling NJ, Delhal J, Vail JR (1984) The geochronology and evolution of Africa. Oxford: Clarendon

Chen H, Stimets RW (2014) Fluorescence of trivalent neodymium in various materials excited by a 785 nm laser. Am Mineral 99: 332-342

Dresselhaus MS, Dresselhaus G, Eklund PC, Chung DDL (1977) Lattice vibrations in graphite and intercalation compounds of graphite. Mater Sci Eng 31:141-152

Fehér F, Laue W, Winkhaus G (1956) Über die Darstellung der Sulfane $H_2S_2$, $H_2S_3$, $H_2S_4$ und $H_2S_5$. Z Anorg Allg Chem 288: 113-122

Fenyrol J, Giuliani G, Demaiffe D, Ohnenstetter D, Fallick AE, Dubessy J, Martelat J-E, Rakotondrazafy AFM, Omito E, Ichang'i D, Nyamai C, Wamunyu AW (2017) Age and origin of the tsavorite and tanzanite mineralizing fluids in the Neoproterozoic Mozambique Metamorphic Belt. Can Mineral 55:763-786

Feneyrol J, Giuliani G, Ohnenstetter D, Fallick AE, Martelat JE, Monié P, Dubessy J, Rollion-Bard C, Le Goff E, Malisa E, Rakotondrazafy AFM, Pardieu V, Kahn T, Ichang D, Venace E, Voarintsoa NR, Ranatsenho MM, Simonet C, Omito E, Nyamai C, Saul M (2013) New aspects and perspectives on tsavorite deposits. Ore Geol Rev 53:1-25

Feneyrol J, Giuliani G, Ohnenstetter D, Le Goff E, Malisa EPJ, Saul M, Saul E, Saul J, Pardieu V (2010) Lithostratigraphic and structural controls of ‘tsavorite’ deposits at Lemshuku, Merelani area, Tanzania. C R Geosci 342:778–785

Fritz H, Abdelsalam M, Ali KA, Bingen B, Collins A S, Fowler, AR, Ghebreab W, Hauzenberger C A, Johnson P R, Kusky TM, Macey P, Muhongo S, Stern RJ, Viola G (2013) Orogen styles in the East African Orogen: A review of the Neoproterozoic to Cambrian tectonic evolution. J Afr Earth Sci 86:65–106

Frost RL, López A, Scholz R, Xi Y, Belotti M. (2013) Infrared and Raman spectroscopic characterization of the carbonate mineral huanghoite - And in comparison with selected rare earth carbonates. J Mol Struct 1051: 221-225

Giuliani G, Dubessy J, Ohnenstetter D, Banks D, Branquet Y, Feneyrol J, Fallick AE (2017) The role of evaporites in the formation of gems during metamorphism of carbonate platforms: a review. Miner Deposita (accepted) https://doi.org/10.1007/s00126-017-0738-4

Giuliani G, Dubessy J, Ohnenstetter D, Banks D, Feneyrol J, Branquet Y, Fallick AE (2015) Le fluide, l'Arlésienne du métamorphisme. Géochronique 136:65-69

Gmelin L (1983) Gmelin Handbook of Inorganic Chemistry, System No. 9, Supplement Vol. 4a/b, Springer-Verlag

Gorbaty YE, Bondarenko GV (1998) The physical state of supercritical fluids. J Supercrit Fluid 14:1-8

Hurai V, Huraiová M, Slobodník M, Thomas R (2015) Geofluids. Elsevier

Hurai V, Paquette J-L, Huraiová M, Slobodník M, Hvoždara P, Siegfried P, Gajdošová M, Milovská S (2017) New insights into the origin of the Evate apatite-iron oxide-carbonate deposit, Northeastern Mozambique, constrained by mineralogy, textures, thermochronometry, and fluid inclusions. Ore Geol Rev 80:1072-1091

Kawashima Y, Katagiri G (1999) Observation of the out-of-plane mode in the Raman scattering from the graphite edge plane. Phys Rev B 59:62-64

Kawashima Y, Katagiri G (2002) Evidence for nonplanar atomic arrangement in graphite obtained by Raman spectroscopy. Phys Rev B 66:104109:1-6

Lafuente B, Downs RT, Yang H, Stone N (2015) The power of databases: the RRUFF project. In: Highlights in Mineralogical Crystallography, T Armbruster and RM Danisi, eds. W De Gruyter, 1-30

Luque FJ, Huizenga J-M, Crespo-Feo E, Wada H, Ortega L, Barrenechea JF (2014) Vein graphite deposits: geological settings, origin, and economic significance. Miner Deposita 49:261-277

Makarov SZ (1933) Löslichkeitsisothermen und Eisfeld im ternären System $Na_2CO_3$-NaCl-$H_2O$. Zeitschrift für allgemeine Chemie III, 2, 234-248 (in Russian)

Martelat J-E, Paquette J-L, Bosse V, Giuliani G, Monie P, Omito E, Simonet C, Ohnenstetter D, Ichang'i D, Nyamai C, Wamunyu A (2017) Chronological constraints on tsavorite mineralizations and related metamorphic episodes in Southeast Kenya. Can Mineral 55**:**845-865 doi: 10.3749/canmin.1700019

Naumov VB, Kamenetsky VS, Thomas R, Kononkova NN, Ryzhenko BN (2008) Inclusions of silicate and sulfate melts in chrome diopside from the Inagli deposit, Yakutia, Russia. Geochem Int 46:554-564

Nemanich RJ, Lucovsky G, Solin SA (1977) Infrared active optical vibrations of graphite. Solid State Commun 23:117-120

Nývlt J (1977) Solid-liquid equilibria. Elsevier, Amsterdam

Oliver BG, Davis AR (1973) Vibrational spectroscopic studies of aqueous alkali metal bicarbonate und carbonate solutions. Can J Chem 51:698-702

Pawley M, Reid A, Dutch R, Preiss W (2015) Demystifying migmatites: an introduction for the field-based geologist. Applied Earth Science 124:147-174

Pohl WL, Horkel A (1980) Notes on the Geology and Mineral Resources of the Mtito Andei-Taita Area (Southern Kenya). Mitt Österr Geogr G 73:135-152

Pohl WL, Nauta WJ, Niedermayr G (1979) Geology of the Mwatate Quadrangle and the Vanadium Grossularite Deposits of the Area (with a Geological Map 1:50,000). Kenya Geol Survey Report No. 101, Nairobi. https://www.researchgate.net/profile/Walter_Pohl

Rankin AH, Taylor D, Treolar PJ (2013) Liquid hydrogen sulphide ($H_2S$) fluid inclusions in unheated tanzanites (zoisite) from Merelani, Tanzania: Part 2. Influence on gem integrity during and after heat treatment. Journal of Gemmology 33:161-167

Reich S, Thomsen C (2004) Raman spectroscopy of graphite. Philos T Roy Soc A 362:2271-2288

Shen AH, Keppler H (1997) Direct observation of complete miscibility in the albite-$H_2O$ system. Nature 385:710-712

Shikin AM, Adamchuk VK, Siebentritt S, Rieder K-H, Molodtsov SL, Laubschat C (2000) Formation of surface graphite monolayer and intercalation like compound in the La/graphite system under thermal annealing. Phys Rev B 61:7752-7759

Suwa K, Suzuki K, Miyakawa K, Agata T (1996) Vanadium grossular from the Mozambique metamorphic rocks, south Kenya. J Southe Asian Earth 14:299–308 http://dx.doi.org/10.1016/s0743-9547(96)00066-9

Tenczer V, Hauzenberger CA, Fritz H, Hoinkes G, Muhongo S, Kloetzli U (2013) Crustal age domains and metamorphic reworking of the deep crust in Northern-Central Tanzania: a U/Pb zircon and monazite age study. Miner Petrol 107:679–707

Tenczer V, Hauzenberger CA, Fritz H, Hoinkes G, Muhongo S, Klötzli U (2011) The P–T–X (fluid) evolution of meta-anorthosites in the Eastern Granulites, Tanzania. J Metamorph Geol 29: 537–560

Thomas R, Davidson P (2012) The application of Raman spectroscopy in the study of fluid and melt inclusions. Z Dtsch Ges Geowiss 163/2:113-126

Thomas R, Davidson P (2016) Revisiting complete miscibility between silicate melts and hydrous fluids, and the extreme enrichment of some elements in the supercritical state — Consequences for the formation of pegmatites and ore deposits. Ore Geol Rev 72:1088-1101

Thomas R, Davidson P (2017) Hingganite-(Y) from a small aplite vein in granodiorite from Oppach, Lusatian Mts, E-Germany. Miner Petrol 111:821–826 https://doi.org/10.1007/s00710-016-0489-4

USGS (2015a) Kenya, Minerals Yearbook 2013. URL https://minerals.usgs.gov/minerals/pubs/country/africa.html#ke

USGS (2015b) Tanzania, Minerals Yearbook 2013. URL https://minerals.usgs.gov/minerals/pubs/country/africa.html#tz

Veksler IV, Thomas R (2002) An experimental study of B-, P- and F-rich synthetic granite pegmatite at 0.1 and 0.2 GPa. Contrib Mineral Petr 143, 673-683

Warren JK (2006) Sabkhas, saline mudflats and pans. In Warren, JK, Evaporites: Sediments, resources and hydrocarbons. Springer Berlin – Heidelberg, Chapter 3, pp 139-220

White RW, Powell R, Halpin JA (2004) Spatially-focused melt formation in aluminous metapelites from Broken Hill, Australia. J Metamorph Geol 22:825–845

Yang H-P, Wen H-H, Zhao Z-W, Li S-L (2001) Possible superconductivity at 37 K in graphite-sulphur composite. Chinese Phys Lett 18:1648-1650

Zhang R, Lehmann B, Seltmann R, Sun W, Li C (2017) Cassiterite U-Pb geochronology constrains magmatic-hydrothermal evolution in complex evolved granite systems: The classic Erzgebirge tin province (Saxony and Bohemia). Geology 45: 1095-1098

Zheng S, Wen Y, Zhu Y, Han Z, Wang J, Yang J, Wang C (2014) In situ sulfur reduction and intercalation of graphite oxides for Li-S battery cathodes. Adv Energy Mater, 1400482:1-9

**Figure captions:**

**Fig. 1** Typical geological setting of massive green vanadium grossular and gem quality transparent tsavorite mineralization at Scorpion mine, SE Kenya, the samples used in this study were taken from a lenticular vein (star) at the face of an incline

**Fig. 2** Green grossular (sample 1) from Kenya, (a) polished section showing graphite-II (Gr-II) and graphite-III (Gr-III) with arzakite (Arz) and calcite (Cal) in garnet. (b) The white circles are the locations of Raman spectra of graphite-II and graphite-III shown below; note the distinct "forbidden" Raman band at 867 $cm^{-1}$

**Fig. 3** Typical Raman spectrum of graphite: (a) graphite-I, (b) graphite-II

**Fig. 4** Unhomogenized melt inclusions in massive green grossular (sample 1) from Scorpion Mine, SE Kenya - (a) a growth zone showing abundant un-homogenized MI. (b) Single sulfur-rich melt inclusion in the same growth zone. The solid components are calcite and several silicate mineral phases. The bubble is mainly $H_2S$-vapor ($H_2S$-v) and traces of $CO_2$. The liquid phase ($H_2S$-l), about 20-30 % (vol/vol) is mainly $H_2S$ and $HS^-$. A globule of native sulfur (S) is also present

**Fig. 5** Rehomogenized melt inclusions in massive green grossular (sample 1) (a) A near critical melt inclusion in green grossular from Kenya after re-homogenization (750 °C, 2 kbar), containing a water-rich silicate glass (G), a fluid (F) and a $H_2S$-bearing vapor phase (V). The bulk water concentration is about 30 % (g/g). (b) A sulfur-rich melt inclusion containing solid sulfur S, liquid $H_2S$ ($H_2S$-l) and $H_2S$ vapor ($H_2S$-v). From the Raman spectra (c) of the fluid phase can be seen that the main components of this phase are $HS^-$ (2570 $cm^{-1}$),

$H_2S$-l (2580 $cm^{-1}$), and $H_2S$ in $CO_2$ (2610 $cm^{-1}$). Both inclusions (a and b) came from the same grossular chip and in close proximity. In the Raman spectrum the strong band at 2570 $cm^{-1}$ is a metastable $HS^-$ band in the liquid $H_2S$ phase, obtained immediately after quenching. At high temperatures $H_2S$ dissolves and reacts in liquid sulfur forming dissolved polysulfanes $H_2S_n$ with n = 2 up to 5, indicated by a strong and broad Raman band at 2500 $cm^{-1}$ (see Fehér et al. 1956). Upon cooling the polysulfanes decompose into sulfur and the primary radical $HS^-$, which we could detect immediately after quenching (see Gmelin 1983). (d) A pseudosecondary plane with hundreds of melt inclusions in green grossular re-homogenized at 750 °C and 2 kbar. (e) a close-up of melt inclusions in the above plane

**Fig. 6** Sulfur-rich melt inclusion in grossular from Kenya (a) photomicrograph of the unheated inclusion, with the associated Raman spectra of (b) native sulfur S and (c) of hydrogen sulfide $H_2S$

**Fig. 7** A typical fluid inclusion in a transparent tsavorite crystal (sample 3) from Tanzania with a REE-carbonate daughter crystal of unknown composition.

**Fig. 8** Raman spectra of green grossular/tsavorite (samples 1, 2, and 3) superimposed with the very strong luminescence lines at 1290, 1452, 1548, and 1846 $cm^{-1}$ (excitation 633 nm). The upper spectrum represents the grossular from Kenya, the middle spectrum crystals from Kenya, and the lower one the spectrum of grossular from a Tanzania nodule

**Fig. 9** The experimentally produced Raman-active 867 $cm^{-1}$ bands in graphite from Sri Lanka. The spectrum labeled La was produced by grinding of graphite with La carbonate, and spectrum labeled Nd by grinding with $NdF_3$. Spectrum (a) is a close up of the 820 to 900 $cm^{-1}$ spectral range in the general spectrum (b), note dashed lines marking this range, showing

peaks at around 867 $cm^{-1}$. In both cases a relatively strong carbonate band at 1088 $cm^{-1}$ was formed in the graphite spectrum, indicating the formation of Nd or La carbonate by tribochemical reaction. The figure 9 intentionally shows schematically, and in slightly exaggerated form, the strong difference of the intense Raman spectra of pure graphite and the very weak intensity of the experimentally produced Raman-active 867 $cm^{-1}$ bands generated by Nd or La carbonate.

**Figures**

**Fig. 1**

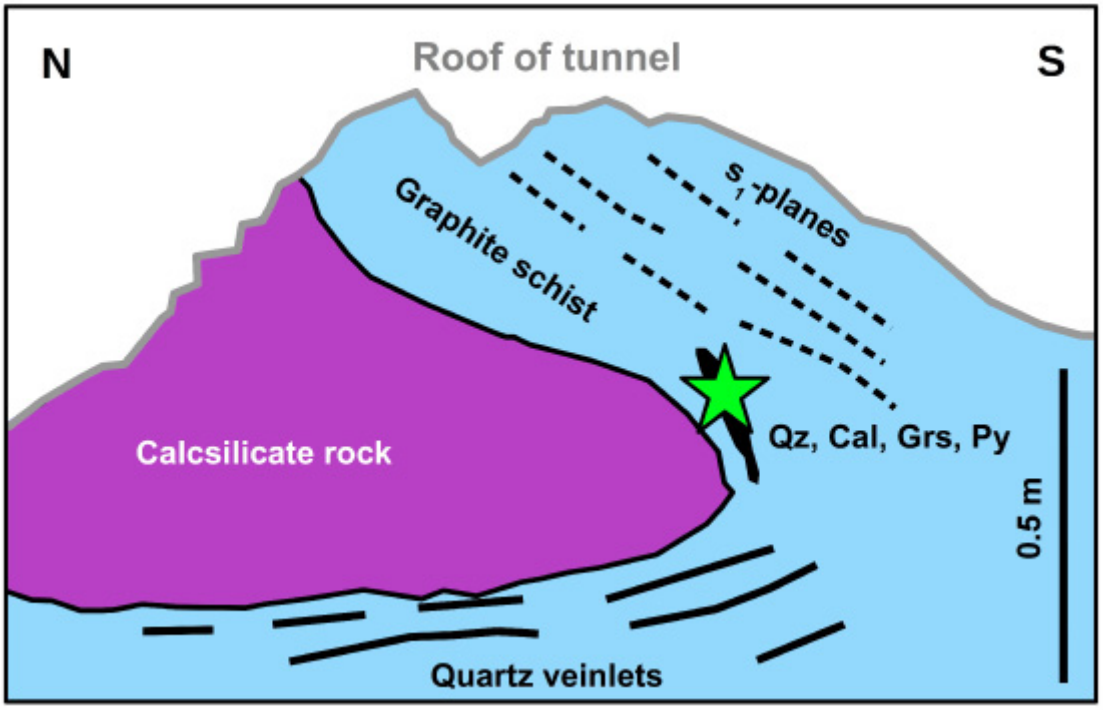

**Fig. 2**

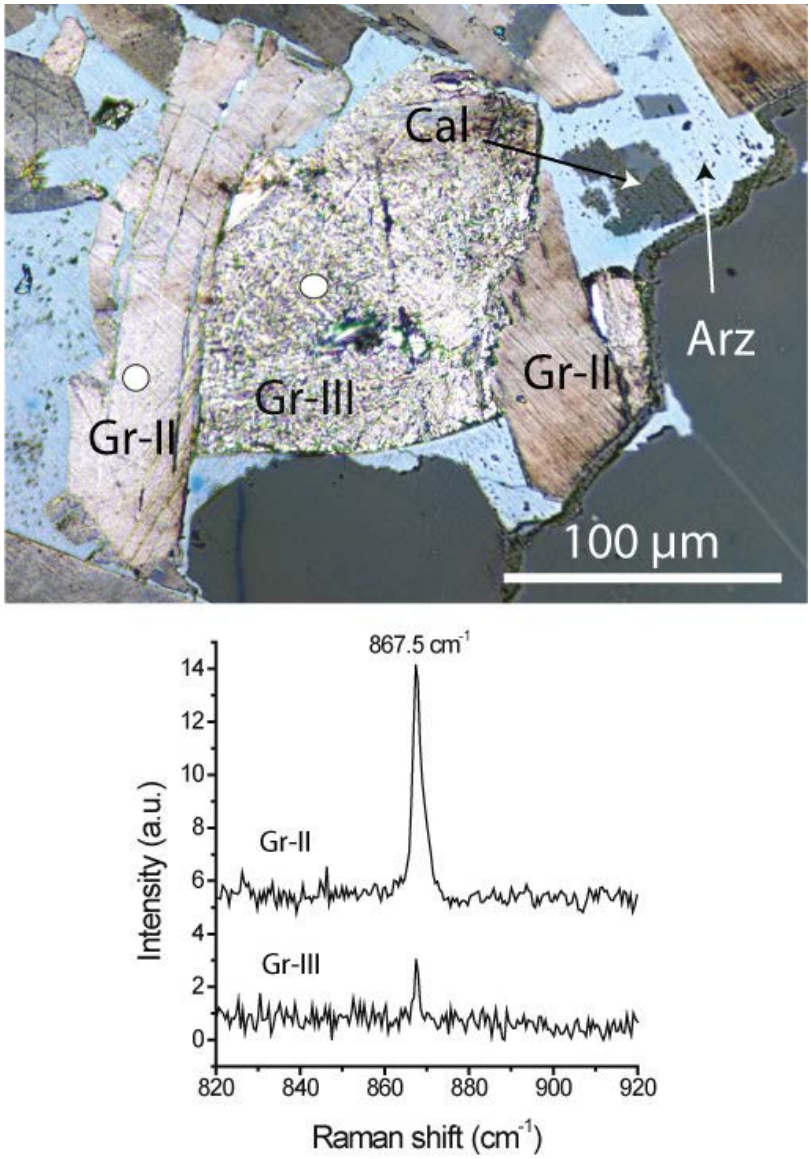
Cal
Arz
Gr-II
Gr-III
Gr-II
100 µm
867.5 cm-1
Gr-II
Gr-III
Intensity (a.u.)
Raman shift (cm-1)
0
2
4
6
8
10
12
14
820
840
860
880
900
920

**Fig. 3**

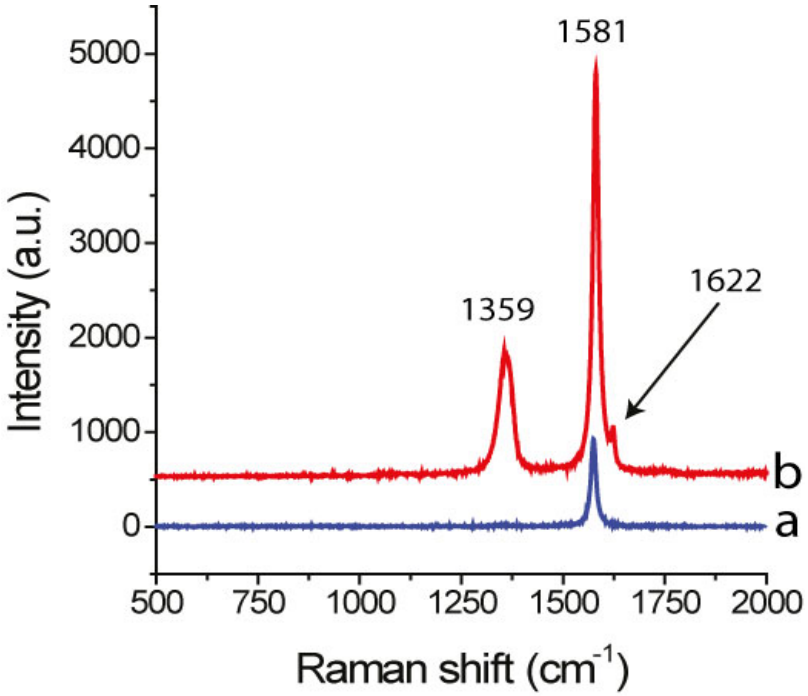
1581
1622
1359
b
a
Intensity (a.u.)
5000
4000
3000
2000
1000
0
500
750
1000
1250
1500
1750
2000
Raman shift (cm-1)

**Fig. 4**

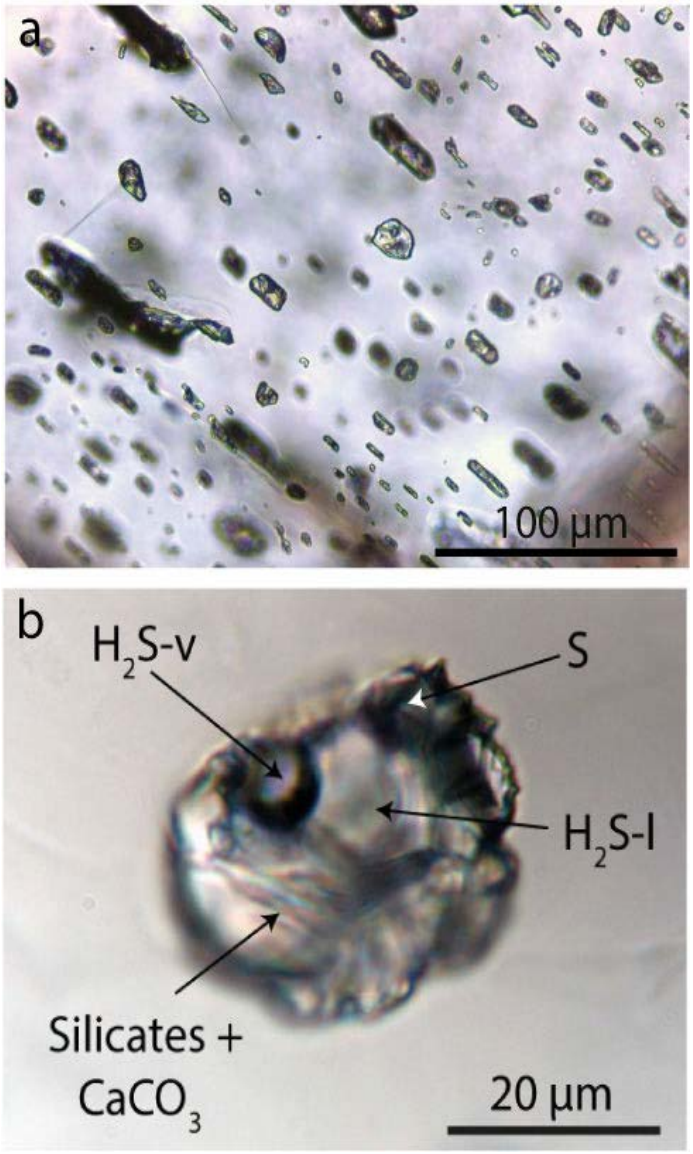

**Fig. 5**

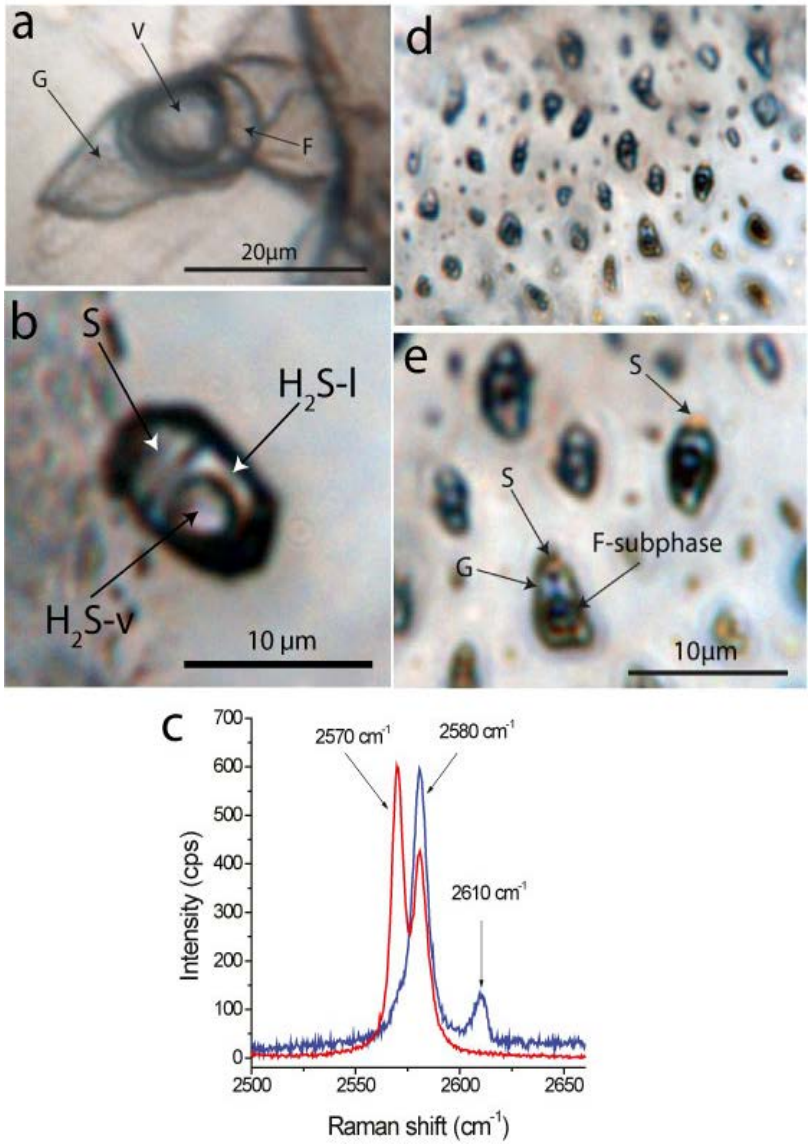
a
V
G
F
20µm
d
b
S
H2S-l
H2S-v
10 µm
e
S
S
F-subphase
G
10µm
c
2570 cm-1
2580 cm-1
2610 cm-1
Intensity (cps)
Raman shift (cm-1)

**Fig. 6**

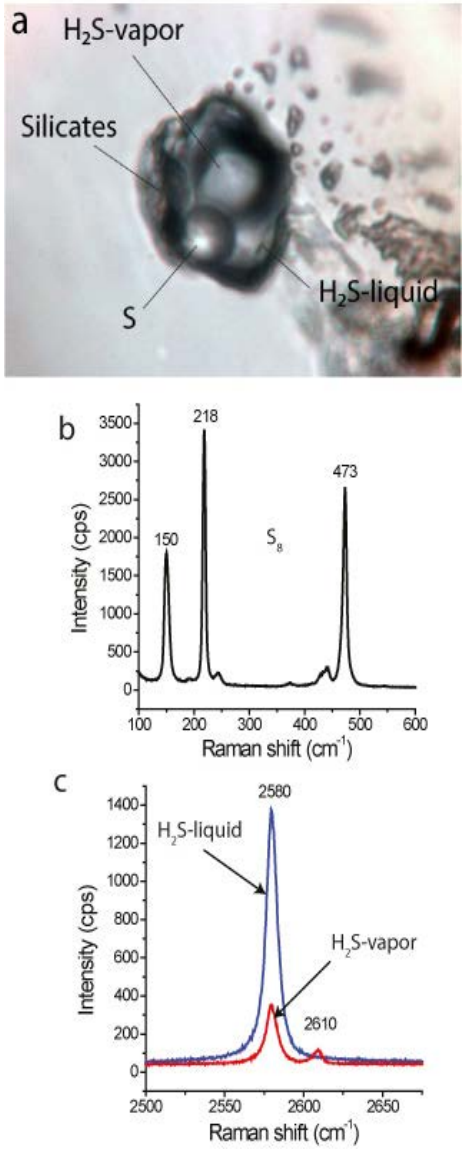
a
H2S-vapor
Silicates
S
H2S-liquid
b
218
473
150
S8
Intensity (cps)
Raman shift (cm-1)
c
2580
H2S-liquid
H2S-vapor
2610
Intensity (cps)
Raman shift (cm-1)

**Fig. 7**

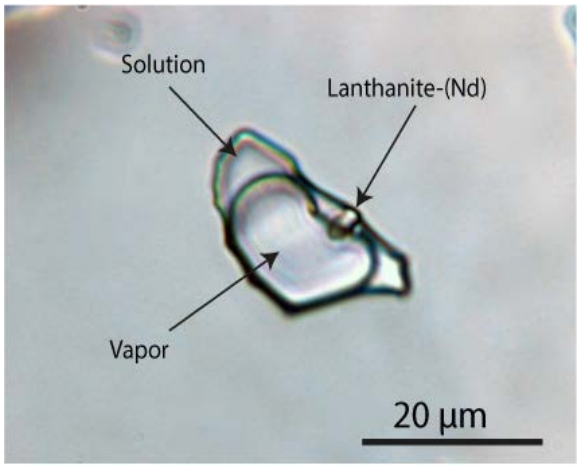
Solution
Lanthanite-(Nd)
Vapor
20 µm

**Fig. 8**

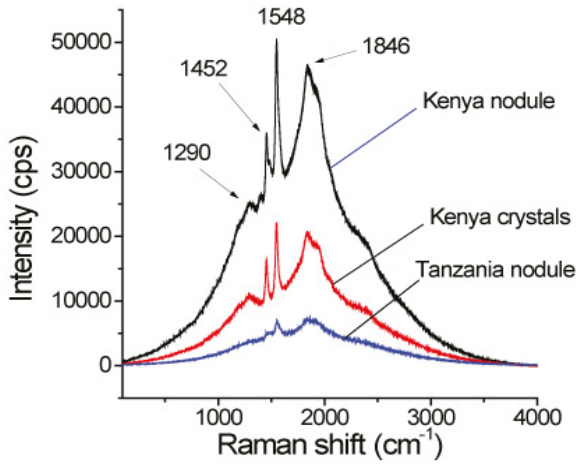
1548
1846
1452
Kenya nodule
1290
Kenya crystals
Tanzania nodule
Intensity (cps)
50000
40000
30000
20000
10000
0
1000
2000
3000
4000
Raman shift (cm-1)

**Fig. 9**

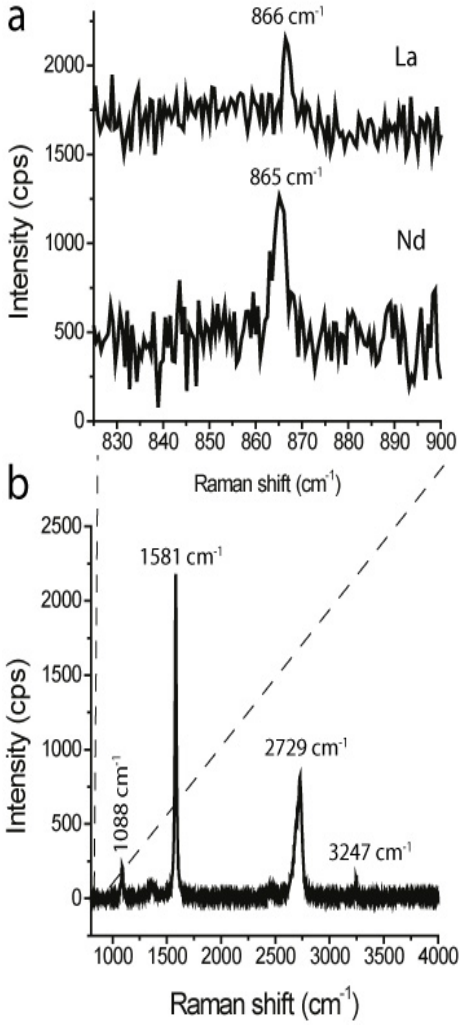
a
866 cm-1
La
865 cm-1
Nd
Intensity (cps)
Raman shift (cm-1)
b
1581 cm-1
2729 cm-1
1088 cm-1
3247 cm-1
Intensity (cps)
Raman shift (cm-1)